Construction and Building Materials 228 (2019) 117071

Contents lists available at ScienceDirect

Construction and Building Materials

journal homepage: www.elsevier.com/locate/conbuildmat

Comparison of corrosion resistance mechanism between ordinary Portland concrete and alkali-activated concrete subjected to biogenic sulfuric acid attack

Yudong Xie, Xujian Lin *, Tao Ji, Yongning Liang, Weijie Pan

School of Civil Engineering, Fuzhou University, Fuzhou 350108, PR China

HIGHLIGHTS

- The corrosion mechanism of AAC and OPC by BSA was investigated.
- The number of bacteria attached to the surface of OPC is higher than that of AAC.
- The main corrosion product of OPC and AAC is gypsum.
- The corrosion of OPC is more serious than that of AAC.

ARTICLE INFO

Article history:
Received 20 July 2019
Received in revised form 4 September 2019
Accepted 23 September 2019
Available online 28 September 2019

Keywords:
Alkali-activated concrete
Biogenic sulfuric acid
Corrosion layer
Bacterial effect

ABSTRACT

The difference of corrosion resistance mechanism between alkali-activated concrete (AAC) and ordinary Portland cement concrete (OPC) under biogenic sulfuric acid corrosion was compared. By measuring the local surface morphology, mass loss, compressive strength and Ca^{2+} dissolution of OPC and AAC specimens, the corrosion resistance of these two kinds of concrete to biogenic sulfuric acid (BSA) was studied. The hydration products and corrosion products of OPC and AAC were studied with X-ray diffraction (XRD), Fourier transform infrared spectroscopy (FT-IR) and environmental scanning electron microscopy-energy dispersive spectroscopy (ESEM-EDS). The results show that under BSA corrosion, the thickness, roughness and porosity of the corrosion layer of OPC are obviously greater than those of AAC. The main corrosion products of OPC and AAC is gypsum. The amount of gypsum produced on the surface of OPC corrosion layer is larger than that of AAC. In addition, the bacterial effect on the surface of AAC corrosion layer is greater than that of OPC, which makes the corrosion path of BSA shorter than that of OPC. Therefore, the corrosion resistance of AAC to BSA is better than that of OPC.

1. Introduction

Microbial corrosion widely exists in all aspects of nature, which is also related to the construction industry, mainly concentrating in sewage treatment facilities, marine buildings and other microbial enrichment areas [1–4]. Microbial corrosion in concrete refers to concrete corrosion caused by microbial metabolism, which can lead to surface damage, surface loosening, mortar shedding, aggregate exposure, cracking and steel corrosion in serious cases as well as shorten the service life of concrete structures. Therefore, it has brought enormous economic losses to mankind. The direct economic loss caused by microbial corrosion is as high as $30–50 billion every year [5]. In the Netherlands, up to 70% of underground materials are corroded by bacteria [6]. 10% to 20% of construction materials in Germany are damaged by microbial corrosion. 10.9% of a 1900 km concrete sewage pipeline in the United States has been corroded by microorganisms, and its maintenance cost is as high as $400 million [3]. For marine buildings, 20% of structural damage and component failure are caused by microbial corrosion in seawater [7].

In 1945, Parker [8] found that BSA was the chief cause of concrete corrosion, and pointed out that the corrosion mechanism of BSA to concrete was that BSA reacted with $Ca(OH)_2$ in concrete to form gypsum. Gypsum can promote the production of ettringite under certain conditions. When ettringite accumulates to a certain amount, it will expand and destroy concrete. At the same time, BSA will make the hydration product C-S-H lose cohesiveness, resulting in the loss of concrete strength [9]. In the past, the mechanism of BSA corrosion of concrete has been widely recognized and cited.

* Corresponding author.
E-mail address: xjl@fzu.edu.cn (X. Lin).

https://doi.org/10.1016/j.conbuildmat.2019.117071
0950-0618/

In recent years, many researchers have carried out a lot of research on the basis of Parker's BSA corrosion mechanism of concrete, and have a new understanding of the corrosion mechanism. When the gypsum layer formed by the reaction accumulates to a certain thickness, the further infiltration of acid can be prevented and the corrosion rate can be reduced [10]. However, Vollersten et al. [2] suggested in their research that the rough surface formed by gypsum could provide a larger corrosion contact area, which was conducive to the continuation of corrosion. In the process of continuous corrosion, reaction between calcium aluminate and gypsum in concrete to generate ettringite, which further accelerates corrosion damage. When the expansion internal stress of ettringite exceeds the tensile strength of concrete, concrete will crack [11,12]. Skalny et al. [13] believed that gypsum could move to the depth of concrete which was not corroded by acid, and then produce stable ettringite under alkaline conditions. However, Davis et al. [14] believed that there was only a small amount of ettringite in the corrosion layer and that ettringite was only an intermediary product. Chen et al. [15] believe that the strength of concrete eroded by BSA decreases because of the formation of expansive gypsum. It can be seen from the above that there are still disputes about the existence and sequence of ettringite and gypsum.

The corrosion of BSA to concrete is affected by many factors. Due to the different hydration products, the reaction mechanism of different types of concrete with BSA is also different. Some studies have shown that the BSA resistance of 35% ordinary Portland cement +65% GBS concrete is much greater than that of sulfate cement concrete [16,17]. In [18], concrete with low porosity and low calcium hydroxide can greatly improve the acid resistance of concrete. Bassuoni et al. [16] pointed out that the corrosion process of sulfuric acid on concrete is determined by aggregate and cementitious materials, and the ion transport path in the corrosive layer is determined by the curvature of aggregate. In addition, the corrosion rate of BSA corroded concrete increased with the increase in BSA concentration [16,19,20].

At present, most of the research focuses on the corrosion of OPC by BSA. Only a few researchers have studied the corrosion mechanism of BSA on other types of cement. Yang et al. [21] found that the dissolution rate of OPC in acid solution is higher than that of sulphoaluminate cement concrete (SAC), and the resistance of SAC to BSA corrosion is much greater than that of OPC. In previous studies [20], it was found that BSA corroded AAC more deeply than CSA. The corrosion products of AAC are not affected by the concentration of BSA, and the main corrosion product is gypsum. Compared with OPC, AAC has better acid resistance and impermeability [22]. Robin et al. [23] found that different types of cement concrete have different properties when corroded by BSA. Jiang et al. [24] soaked the alkali slag cement concrete test block in a different acid solution of 5% concentration for 6 months. It was found that the compressive strength of the test block immersed in the citric acid did not change, the strength of the test block immersed in hydrochloric acid and nitric acid was moderately decreased, while the strength of the test block soaked in sulfuric acid was markedly decreased. Sun et al. [25] found that soaking alkali fly ash cement slurry in sulfuric acid solution would cause damage to concrete surface. Yang et al. [21] found that the variation of compressive strength, mass loss rate and appearance corrosion degree are higher for OPC than those of SAC exposed to BSA.

From the above analysis, it can be concluded that the application of AAC in marine, sewage pipeline and other areas corroded by BSA has good prospects. However, on the premise that the mechanical properties of AAC and OPC are basically the same, the different BSA corrosion mechanism of AAC and OPC in seawater has not been studied. In order to provide as much useful information (especially in marine applications) as possible for the mechanism of BSA corrosion of concrete, it is necessary to compare the corrosion resistance mechanism between OPC and AAC under BSA attack. In this context, the main purpose of this paper is to preliminarily understand the BSA corrosion resistance and its mechanism of AAC and OPC. Thus, the corrosion resistance of BSA on AAC and OPC was studied in terms of surface morphology, compressive strength and calcium leaching amount. The difference of corrosion mechanism between OPC and AAC was analyzed with XRD, ESEM-EDS and FT-IR.

2. Materials

The content of chemical composition of fly ash and slag is shown in Table 1, which provided by Fuzhou Shuangteng Building Materials Co., Ltd. Analytical Reagent produced by Tianjin Zhiyuan Chemical Reagent Co., Ltd., the content of NaOH is not less than 96%. In this study, ordinary Portland cement (P·O 42.5) was used, and the compressive strengths of 3 and 28 days were measured at 27.5 MPa and 45 MPa, respectively. Table 2 shows the performance indexes of river sand, which were measured according to GB/T14684-2001 [26]. Select ordinary stones according to GB/T14685-2001 [27]. Polycarboxylic acid retarder (KDSP-1) with water reducing rate of 25% was used. Tap water in Fuzhou area (China). T.f Bacteria was provided by Xiamen Institute of Oceanography. A medium solution used to simulate BSA corrosion contained 1000 ml H_2O, 44.78 g $FeSO_4{\cdot}7H_2O$, 0.01 g $Ca(NO_3)_2$, 0.5 g $MgSO_4{\cdot}7H_2O$, 0.5 g K_2HPO_4, 0.1 g KCl and 3 g $(NH_4)_2SO_4$. The chemical composition of seawater contained 23.467 g/L NaCl, 4.981 g/L $MgCl_2$, 3.917 g/L Na_2SO_4, 1.102 g/L $CaCl_2$, and 0.664 g/L KCl.

3. Experimental

3.1. Selection of strains

As the main acid-producing bacteria, sulfur-oxidizing bacteria is mainly divided into acidophilic sulfur-oxidizing bacteria (ASOM) and neutral sulfur-oxidizing bacteria (NSOM), and mainly produce acid by ASOM [8]. According to Berger's Bacterial Identification Manual [28], both NSOM and ASOM are strictly autotrophic aerobic bacteria. NSOM is suitable for growth in neutral alkaline medium with pH ranging from 6.0 to 8.0. The representative bacteria are Thiobacillus thioparus and Thiobacillus neapolitanus.

ASOM is suitable for growth in acidic medium with pH ranging from 1.0 to 3.5. It represents the bacteria Thiobacillus thiooxidans (T.t) and Thiobacillus ferrooxidans (T.f). In the midst of process of BSA corrosion of concrete in nature, neutral sulfur oxidizing bacteria NSOM first attaches to the surface of concrete and produces sulfuric acid, which reduces the surface pH value of concrete to less than 3.5. After that, the ASOM (acidophilic bacteria) began to grow and produced a large amount of sulfuric acid, which further corroded the concrete structure, and the pH value dropped below 1.0 [29], however, this process is very long. In order to accelerate the test, H_2S can be quickly converted into sulfuric acid to decorrod concrete by immersing the specimen in acidic medium (initial pH = 2.5) with T.f bacteria added. In this paper, T.f was used as acid-producing bacteria to simulate the corrosion of AAC and OPC. In this experiment, T.f was cultured on 9 K medium. The color of 9 K liquid medium changed from light green to light yellow and then to yellow brown, as shown in Fig. 1. After 3 days of shaking culture, many short rod-shaped T.f bacteria, about 1.0–2.0 mm in length and 0.3–0.5 mm in width, can be clearly seen with electron microscopy (1000 times), as shown in Fig. 2.

3.2. Sample preparation

According to the requirements of the test, the proportion of AAC was designed according to the proportion design method of C60 [30]. The proportion of OPC and AAC is shown in Table 3. To prepare the OPC sample, cement, ordinary stone and river sand were first stirred at a low speed for 1 min in a blender, and then a pre-

Table 1
Chemical composition (% wt.).

No	Al_2O_3	SiO_2	MgO	Fe_2O_3	TiO_2	Na_2O	SO_3	CaO	LOI
Fly ash	24.96	50.02	1.47	4.46	1.57	0.78	1.06	7.52	4.01
Slag	13.01	32.85	10.78	0.29	2.15	0.32	1.91	37.44	0.2

Table 2
Performance index of the river sand.

Bulk density (kg/m^3)	Fineness modulus	Water absorption (%)	Mud Content (%)	Apparent density (kg/m^3)
1480	2.5	0.1	3.53	2591

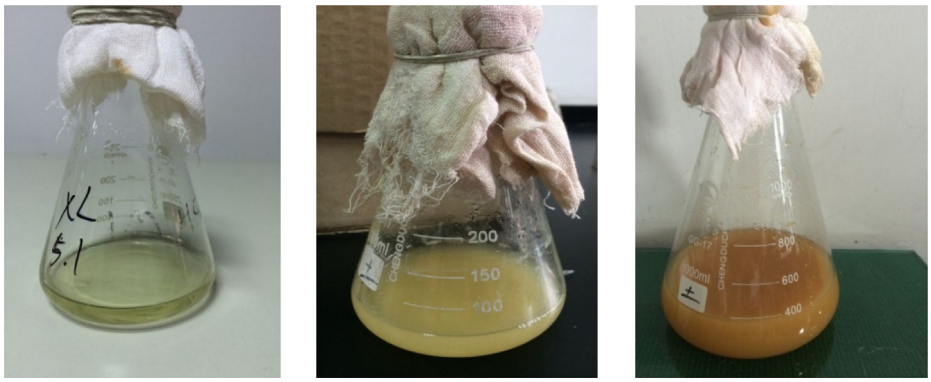

Fig. 1. Changes in color of bacterial medium during oscillating culture.

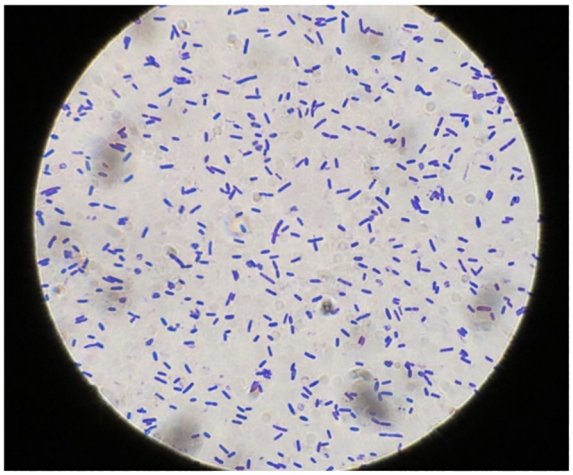

Fig. 2. T.f bacteria under electron microscope (1000 times).

configured superplasticizer (SP) solution was added and fully stirred for 2 min. The mixture was then poured into a greased mold (100 mm × 100 mm × 100 mm) on the inner surface and compacted carefully to minimize the amount of air retained in the mold. After standard curing for one day, the mold was removed, and then the test block was put into seawater (rather than fresh water, because in order to better simulate microbial corrosion in marine environment) for curing for 27 days. After repeated experiments, the chlorides in the seawater does not change the corrosion mechanism of concrete without steel rebar. To prepare the AAC sample, fly ash, slag, river sand and ordinary stone were first stirred at a low speed for 1 min in a blender, and then preconfigured NaOH solution was added and fully stirred for 1 min. The mixture was then poured into a greased mold (100 mm × 100 mm × 100 mm) and compacted carefully to minimize air retained in the mold. Then cover the sample with plastic film for 24 h (20 ± 2 °C, RH > 80%), and remove the mold, and put the test block into the autoclave equipment (Firstly, vacuum pump pumping for 30 min, then raise the temperature to 195 °C and the pressure to 1.2 MPa for 1 h, then lower the pressure for 2 h). Subsequently, the test block was placed in seawater at a constant temperature (20 ± 2 °C) for curing for 27 days. All test blocks should be moved into the ventilation room for 2 days before the BSA corrosion test on AAC and OPC with the BSA corrosion simulation device. All the corrosion times mentioned in the following test steps are timed from the time when the test block is put into the BSA corrosion simulation device. Table 4 shows the initial workability and mechanical properties of AAC and OPC.

Table 3
Mix proportion of AAC and OPC (kg/m^3).

No	Cement	Water	NaOH	Fly ash	Slag	River sand	Stone	SP
OPC	500	170	–	–	–	527	1233	1.4%
AAC	–	170	38.51	92.30	369.19	527	1233	–

Table 4
Initial performance of AAC and OPC.

No	Slump (mm)	Expansion (mm)	Quality (kg)	28-day Compressive strength (MPa)	Average pore size (nm)
AAC	110	170	2.410	65.5	17.5
OPC	250	580	2.405	59.1	31.3

3.3. Biogenic sulfuric acid corrosion simulator

Simulation and study of the process of microbial corrosion of concrete was conducted in different laboratories. Sand et al. [31] built a microbial corrosion laboratory and measured corrosion rates based on mass loss of concrete specimens. Mori et al. [32,33] built laboratories to simulate microbial corrosion of concrete; they determined corrosion rates by measuring decreases in the cross section of mortar samples. In our previous work, we designed a device to simulate the corrosion of concrete by BSA, as described in [21], and the pH value of the medium ranged from 1.0 to 2.5 (more than 1.0, see [21]). Therefore, three different sulfuric acid concentrations (pH = 1.1, 1.6 and 2.0) were designed to analyze the effect of different BSA concentrations on the corrosion mechanism of concrete.

In order to obtain different bacterial liquid with pH values (pH = 1.1, 1.6 and 2.0) during the experiment to consider the influence of different bacterial growth conditions on the test block, the corrosion experiment was conducted by only changing H_2S concentration and keeping other parameters unchanged. According to Fig. 3 [21], a small scale BSA corrosion simulator without test blocks was fabricated as is shown in Fig. 4, and the specific parameters such as H_2S concentration and oxygen flow rate were determined by the device. After many experiments, the following concentration was finally determined as the experimental conditions:

For 250 ml bacterial solution, the inoculation amount of bacteria was 10%, the room temperature was 25 °C, the oxygen flow rate remained unchanged (30 ml/min), and the flow rate of HCl and Na_2S was 1.4 ml/min. Bacterial solution with pH = 1.1 was obtained by 0.0856 M of Na_2S and 0.0422 M of HCl (the concentration of H_2S was 650–750 ppmv); bacterial solution with pH = 1.6 was obtained by 0.0428 M of Na_2S and 0.0211 M of HCl (the concentration of H_2S in 300–450 ppmv was 300–450 ppmv); bacterial solution with pH = 2.0 could be obtained without introducing HCl and Na_2S. Fig. 5 is the measured pH curve of bacterial solution under three conditions. The medium solution used in the experiment was changed and adjusted every 14 days.

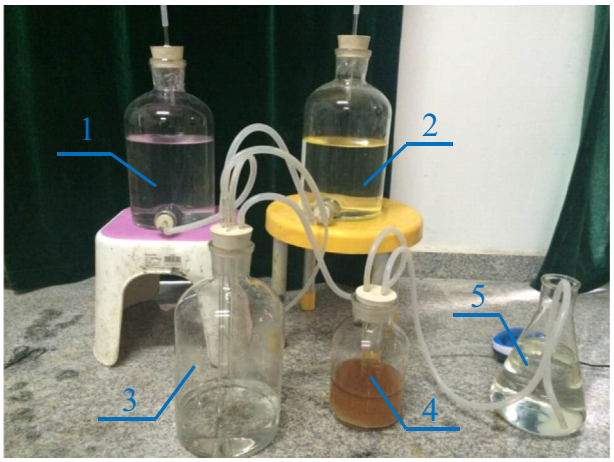

Fig. 4. Simulated BSA corrosion device without specimens, 1-Na_2S solution, 2-HCl solution, 3-H_2S reaction bulb, 4-Medium erosion liquid, 5-Water.

In the test results below, SA1.1, SA1.6 and SA2.0 stand for the corrosion of AAC samples in BSA solutions with pH values of 1.1, 1.6 and 2.0, respectively. SP1.1、SP1.6 and SP2.0 stand for the corrosion of OPC samples in BSA solutions with pH values of 1.1, 1.6 and 2.0, respectively. SA1.1–5 means that AAC sample is taken

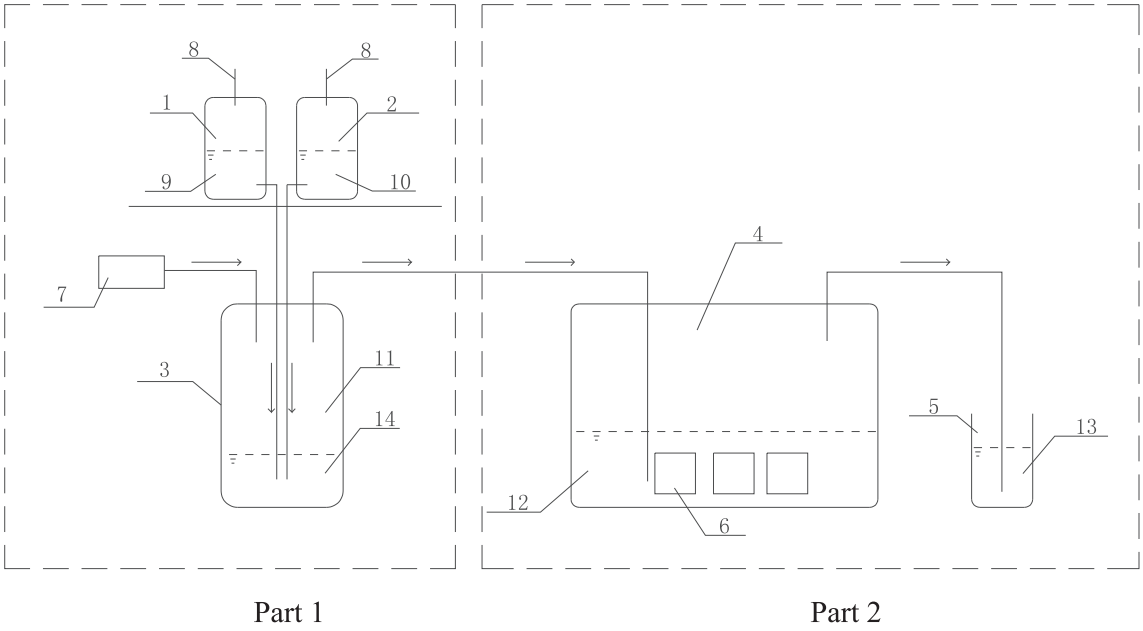

Fig. 3. Setup of the BSA corrosion tests (adapted from [21]), 1-Na_2S bottle, 2-HCl bottle, 3-H_2S reaction bulb, 4-Bacteria cultured medium, 5-H_2S absorption bottle, 6-Specimen, 7-Oxygen pump, 8-Flow control valve, 9-Na_2S solution, 10-HCl solution, 11-H_2S and air mixture, 12-Medium erosion liquid, 13-Zinc acetate solution, 14-Water.

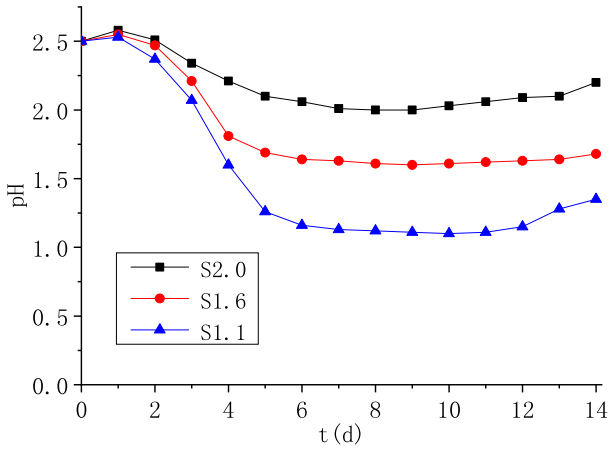

Fig. 5. pH value of cultured medium in function of time [20].

from a depth of 5 mm from the sample surface. SP1.1–5 means that OPC sample is taken from a depth of 5 mm from the sample surface.

3.4. Test methods

3.4.1. The appearance and quality of concrete are changed after BSA corrosion

The most straightforward way to determine the degree of corrosion of concrete by BSA is to observe changes in the appearance and quality of the test block. The surface color of the specimen will change, the surface will peel off, the corrosion layer will be formed on the surface and the aggregate will be exposed under the BSA corrosion. These appearance changes provide the most direct basis for studying the law of BSA corrosion of concrete. In this paper, the EOS 6D digital camera produced by Canon Company is used to record the appearance changes of concrete blocks. In order to reduce the error of test analysis, the distance between the surface of each sample and the camera lens was maintained at 50 cm.

After soaked in a predetermined period, removed the soft layer of the surface with a brush, and then dried in a cool place with a clean cloth, and then dry in an oven at 40 °C constant temperature for 24 h. Then the mass of the test block is weighed and the weight loss rate of the test block is calculated.

The mass loss rate of concrete is calculated according to Eq. (1):

$$m\% = \frac{m_t - m_0}{m_0} \times 100\% \quad (1)$$

In Eq. (1), m_0 represents the mass of samples before corrosion (g); m_t stands for the mass of samples at different ages under BSA corrosion (g); $m\%$ is the percentage of mass loss of concrete blocks.

3.4.2. Compressive strength and Ca^{2+} emission

The test method of compressive strength is carried out according to the Chinese Code GB/T50081-2002 [34], three samples were prepared for each compressive strength measurement. The determination method of Ca^{2+} release from concrete is adopted from [20].

3.4.3. XRD, FT-IR and ESEM analyses

The local morphology of corrosion products near the surface of the samples was observed with XL30 environmental scanning electron microscopy (ESEM-TMP). FT-IR and XRD were used to analyze the hydration products of OPC and AAC before and after BSA corrosion. After the concrete was broken at the required age, the corrosion specimens collected from 5 mm away from the surface of concrete were placed into an agate mortar for grinding, and then the samples were passed through a 0.075 mm sieve. With the use of Nicolet 360 intelligent infrared spectrometer, FT-IR spectra of specimens were recorded in the wavenumber range of 400–4000 cm^{-1}. X/Pert Pro MPD X-ray powder diffractometer (XRD) produced by Philips Corporation of the Netherlands. Cu Kα radiation was used in the 2θ range of XRD between 5°and 80°, with a step length is 0.02° and 2 s/step count time.

4. Results and discussion

4.1. Appearance change

For the BSA corrosion of OPC, Monteny et al. [11] considered that the main corrosion products are gypsum and ettringite, which cover a loose layer on the surface of the corrosion layer of the test block. The porosity of this layer grows with time and provides good living conditions for bacteria. Due to the increasing porosity of the layer, bacteria can penetrate into the deeper layer of concrete through the pores, causing corrosion of the test block by sulfuric acid. They also believe that the moist environment of gypsum provides a good breeding base for bacteria, accelerating the growth of bacteria as well as the rate of corrosion.

Fig. 6 shows the appearance change of AAC and OPC under the action of BSA. It can be concluded that the surface layer of SA1.1 peels off at the 84 days, the coarse aggregate is exposed, and a

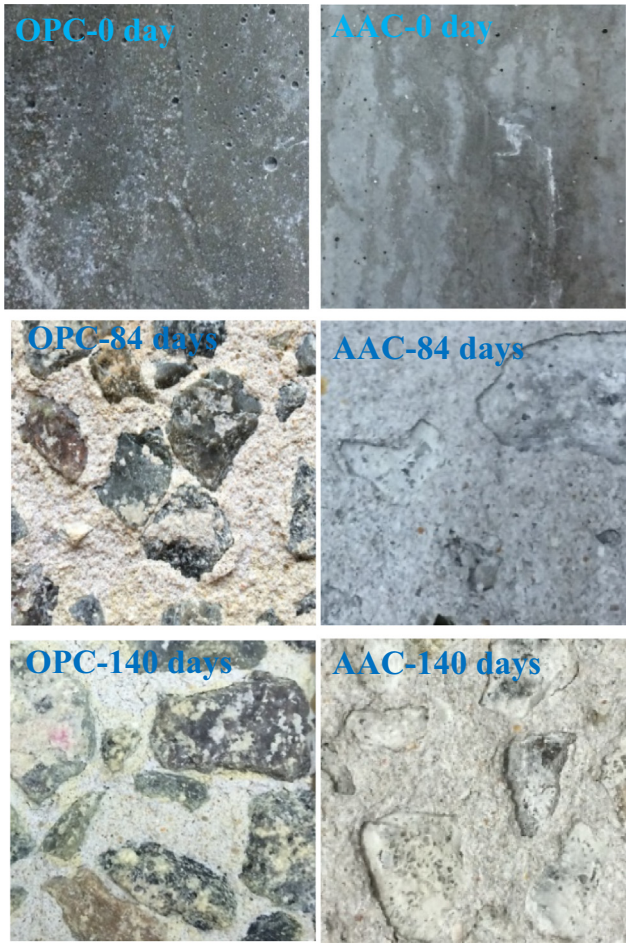

Fig. 6. Appearance images of AAC and OPC attacked by BSA at the 0, 84th and 140th day in the case of pH = 1.1.

gap between the aggregate and the mortar exists; the aggregate protruded 3 mm from the corroded surface at 140 days, and the existence of a gap between the aggregate and the mortar is clear. At 84 days of the SP1.1, a large piece of coarse aggregate was exposed, and the aggregate protruded from the surface of the test block by 3 mm; the aggregate protruded from the test block by 5 mm at 140 days. Both AAC and OPC start to change color to whitish from black ash, which may be due to the formation of gypsum. However, the AAC is off the gray paste, and the OPC is off the white paste. Also, the amount of gypsum produced by AAC is less than that of OPC, so the color is similar to the matrix as gray-black paste. And OPC is white because of the large amount of gypsum.

In this experiment, the gypsum layer of OPC is obviously soft, the surface roughness is large, and the pores are relatively large, which is more conducive to the infiltration of SO_4^{2-} and the dissolution of Ca^{2+}. Therefore, the living environment of SP1.1 is better than that of SA1.1, and the accelerated corrosion ability of bacteria should be stronger. In addition, OPC contains more $Ca(OH)_2$, which reacts with acid as soon as it contacts [35], resulting in OPC itself unable to resist acid erosion. Thus, OPC is much more affected by bacteria than AAC and is subject to more severe corrosion.

4.2. Mass change

As shown in Fig. 7, the increase in BSA concentration only raise the loss rate of concrete mass, and has no effect on the corrosion rule, regardless of OPC or AAC. Therefore, the following analysis focuses on the causes of mass loss of AAC and OPC at pH = 1.1. For SA1.1, the mass loss rate was 1.78% on the 28th day and 13.1% on the 140th day. For SP1.1, the mass loss rate was 1.9% on the 28th day and 20% on the 140th day. Thus, the mass loss rate of SP1.1 at 140 days is 1.52 times that of SA1.1, that is, AAC is more resistant to BSA corrosion than OPC. In the section of appearance change, we know that the production of gypsum in OPC is larger than that in AAC because of the existence of $Ca(OH)_2$ in OPC. This results in bacteria producing more BSA on the surface of OPC than AAC. Moreover, the corrosion rate of concrete increases with the increase of BSA concentration [16,19]. Therefore, the mass loss rate in OPC is higher than that in AAC.

4.3. Ca^{2+} emission

It can be seen from Fig. 8 that the initial release of calcium ions is low because the surface of the concrete has not softened and the bacteria has an environmentally accommodating process.

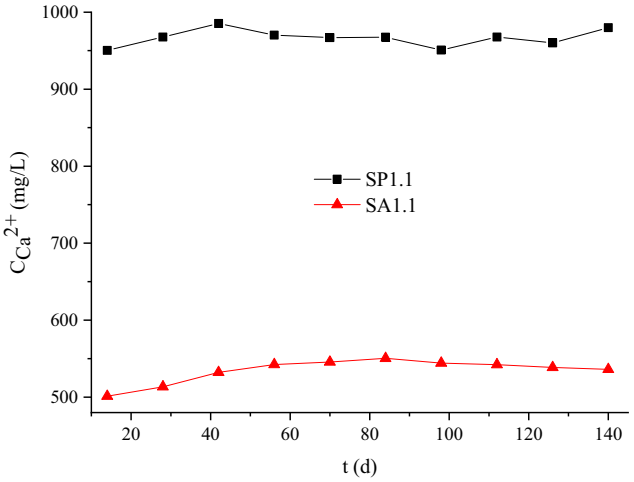

Fig. 8. The Ca^{2+} emission of AAC and OPC corroded by BSA.

However, after the bacteria adapt to the living environment, the release of Ca^{2+} is significantly increased, maintaining at a stable level. For SA1.1, it can be seen that the concentration of calcium ions is maintained at about 530 mg/L, and the change in the curve is small. For SP1.1, it was found that the concentration of calcium ions was maintained at a high level throughout the range of 960 mg/L. The amount of calcium ion released by SP1.1 was 1.81 times that of SA1.1. This is because AAC produces less gypsum than OPC, and bacteria have few effects on AAC; The OPC generates more gypsum, which provides favorable conditions for the growth of bacteria and damages the internal structure. Therefore, the release is increased by one level. This is consistent with the low calcium and acid resistance of AAC itself.

4.4. Variation of compressive strength

As shown in Fig. 9, whether OPC or AAC, the decrease of pH value of corrosive solution only increases the loss rate of compressive strength of concrete. This is because with the increase in BSA concentration, the amount of Ca^{2+} dissolves, the amount of gypsum is produced and the bacterial effect increases. However, the concentration of BSA has no effect on the regularity of corrosive concrete. The difference between SA1.1 and SP1.1 is highlighted below: For SA1.1, the initial strength is 65.5 MPa, the 20 weeks strength is 42.92 MPa, and the strength loss is 34.47%; for SP1.1,

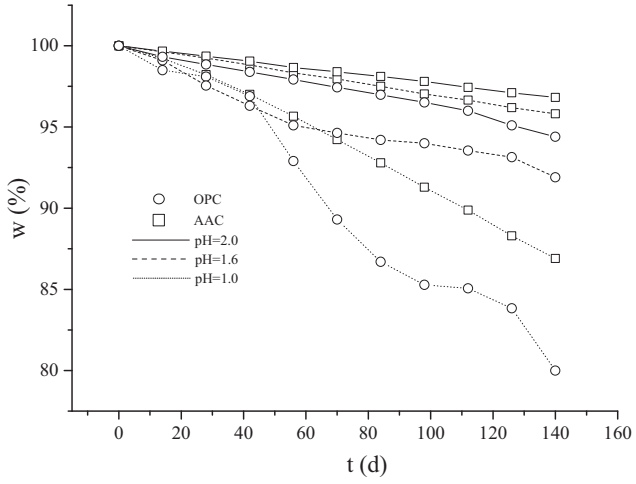

Fig. 7. Mass change of AAC and OPC under the attack by BSA.

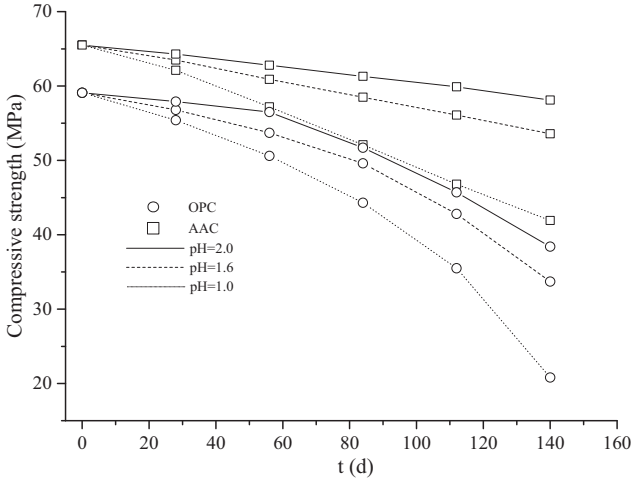

Fig. 9. The compressive strength of AAC and OPC corroded by BSA.

the 8 weeks is 50.6 MPa, the strength loss is 14.38%, and the average weekly loss is 1.79%. The strength at the 20 weeks is 20.8 MPa, and the strength loss was 64.8%. The compressive strength loss of SP1.1 is 30.33% larger than that of the SA1.1 group. Therefore, the internal damage degree of SP1.1 is larger than that of SA1.1. This is consistent with the conclusion of the section on appearance analysis.

4.5. ESEM analysis

4.5.1. The distribution of bacteria and the condition of the corrosion layer

According to the results observed by previous electron microscope (Fig. 2), white lines are used to frame the areas with attached bacteria in Fig. 10(a) which schematically illustrates the distribution of bacteria on AAC and OPC surfaces. Obviously, the number and area of bacteria in the areas with attached bacteria shows that the number of bacteria on the surface of OPC is higher than that on the surface of AAC. It can be found that the distribution of bacteria on the surface of the specimen is not uniform, but clustered together showing an uneven cluster distribution. Fig. 10(b) shows the situation in which the bacterial mass is magnified 3000 times. It can be found that T.f bacteria is long columnar, with a size range of 0.5–3.0 μm. This result is consistent with what observed under electron microscope, so the material in the white wireframe in Fig. 10(a) is confirmed as T.f bacteria.

In Fig. 11(a), there is a gypsum layer of about 1.7 mm thick in SA1.1, and the internal structure remains intact except for the corrosive layer, without cracks or signs of looseness. Fig. 11(b) shows the corrosion layer of the gypsum surface of SP1.1. It can be seen that not only is the gypsum layer loose, but also the area behind the gypsum layer is a bit loose, and the cracks are randomly distributed, that is, the internal structure of the OPC is destroyed. Moreover, the corrosion layer thickness of SP1.1 is obviously larger than that of SA1.1.

Fig. 12(a) is the variation of the element contents in the corrosion zone of AAC after being corroded by BSA. In SA1.1, there are more S elements in the area of 0–2 mm, and no S elements are found in the area of more than 2 mm. S elements are probably derived from gypsum produced by corrosion layer. Calcium content is relatively low in the 0–3.3 mm area, which is due to the dissolution of calcium elements after the corrosion of hydrated calcium silicates. For Si and Al elements, it is found that the content of Si element is low in 0–0.5 mm and Al is low in 0–2 mm. This is because the surface of concrete is softened, the Si-O and Al-O bonds have been severely damaged, and the elements of Si and Al are dissolved. In addition, the dissolution depth of Al is deeper than that of Si, which probably because the fact that $[AlO_4]^{5-}$ tetrahedron is easier to dissolve than $[SiO_4]^{4-}$ tetrahedron.

Fig. 12(b) is the variation of the element contents in the corrosion zone of OPC after being corroded by BSA. In SP1.1, the content of S elements (from gypsum) in the range of 0–5 mm is relatively high, which indicates that OPC is more corroded by BSA than AAC. In the range of 0–5 mm, the content of calcium is relatively low, which indicates that most of the hydrated calcium silicates are destroyed, which leads to the dissolution of calcium. In addition, the content of Al and Si elements decreases gradually from the inside to the outside, which can be considered that Al and Si elements dissolved by H^+ have been leached into the external solution. However, in AAC, the contents of Si and Al are higher in the range of 0.5–5 mm and 2–5 mm, respectively, this indicates that the Si-O and Al-O bonds have not been destroyed. It could be inferred that AAC is more resistant to the corrosion of biological sulfuric acid than OPC.

In brief, the thickness, roughness and porosity of the corrosion layer produced by BSA corrosion of OPC are obviously greater than that of AAC. May be the bacterial effect of OPC corrosion layer is greater than that of AAC, which shortens the path of BSA corrosion of OPC. Therefore, the BSA corrosion of OPC is much greater than that of AAC.

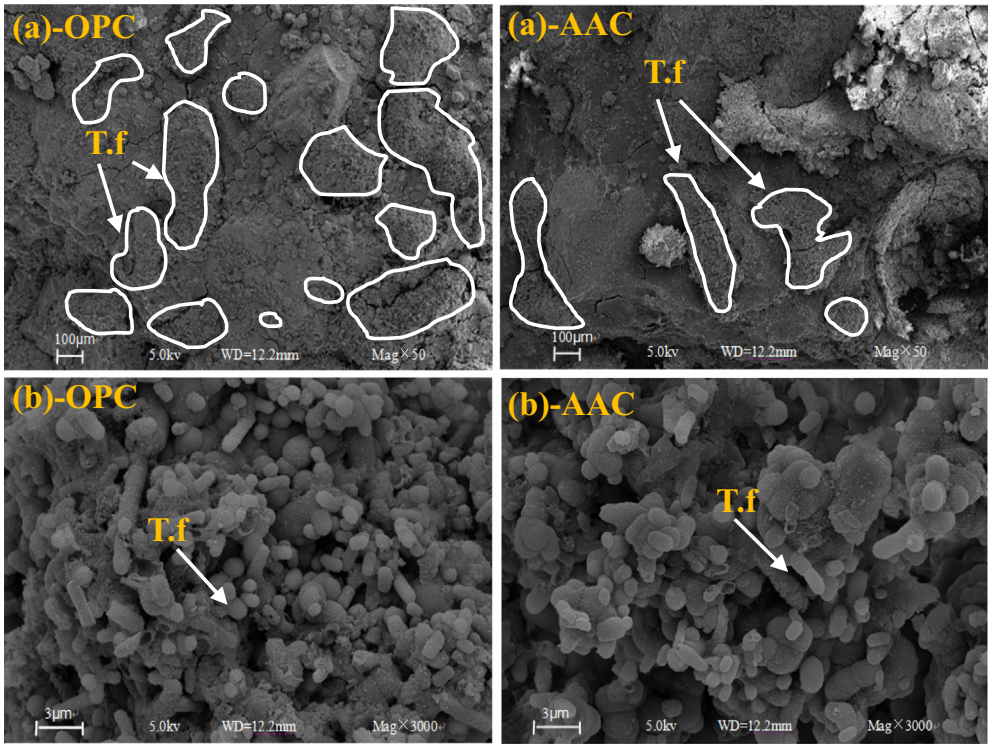

Fig. 10. The bacterial attachment on the surface of OPC and AAC: (a) Distribution of bacteria; (b) The morphology of bacteria.

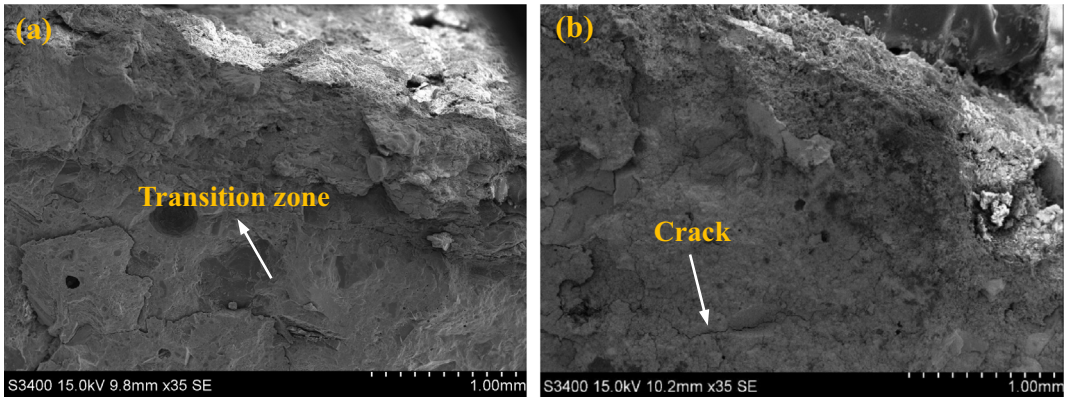

Fig. 11. Corrosion layer of AAC and OPC under BSA corrosion: (a) SA1.1; (b) SP1.1.

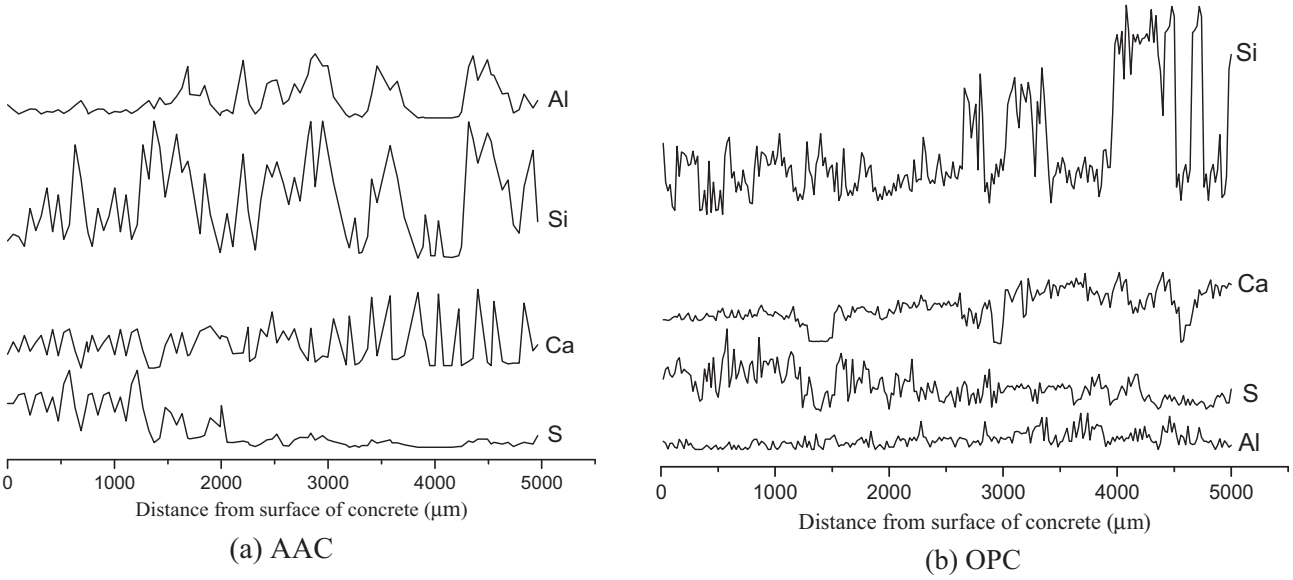

Fig. 12. The EDS spectrum of the distribution of elements of concrete corrosion products attacked by BSA.

4.5.2. Corrosion products

Based on the above our previous analysis [20,21], the hydration products of AAC before corrosion are mainly Xonotlite, Tobermorite, C-S-H (B) and other hydrated calcium silicate materials, while the aluminosilicate is mainly Gmelinite. $Ca(OH)_2$ and C-S-H are the main hydration products of OPC.

Fig. 13 shows the corrosion morphology of AAC. In Fig. 13(a), the Xonotlite is fused with gypsum; Fig. 13(b) shows that the surface of the Zeolite is covered with a layer of gypsum; Fig. 13(c) shows that the entire wall of the hole is covered with gypsum, the crystal shape of the gypsum is clearly visible, and the product at the original hole wall is swallowed by gypsum. It can be obtained that the calcium ions generated by the decalcification reaction of the Xonotlite after being corroded by the BSA combine with the invading SO_4^{2-} to form gypsum; Aluminosilicate-based substances such as Zeolite cause dissolution of aluminum ions due to corrosion of BSA, causing structural damage and loss of the original crystal shape. The Zeolite particles are eventually also covered by gypsum, which is the most important corrosion product.

Fig. 14 shows that the corrosion layer of OPC contains a large number of well-formed and regular-shaped gypsum crystals; the walls of the holes in the holes are covered by large pieces of gypsum.

By comparing the morphology of OPC and AAC attacked by BSA, we can find that the most important corrosion product of both is gypsum. The degradation occurring in the binder system and precipitation of gypsum is cause by the presence of calcium rich gel phase (C-S-H) and $Ca(OH)_2$ in OPC [36]. On the other hand, there is no aluminosilicate such as Al-Tobermorite or Gmelinite in OPC, which is one of the major differences between OPC and AAC. Due to the effect of bacteria, the content of aluminum can inhibit the growth and reproduction of bacteria [37]. In addition, the content of gypsum on the surface of OPC is more than that of AAC, and the humid gypsum environment provided by OPC is superior to the one provided by AAC, which results in bacteria preferring to survive and reproduce on the surface of OPC. Therefore, the number of bacteria adsorbed on the surface of AAC can be much smaller than that of OPC, which leads to the dissolution rate of OPC is higher than that of AAC under the BSA attack.

4.6. X-ray diffraction

Fig. 15 shows the XRD pattern after BSA corroded AAC and OPC. Compared with Fig. 15(a) and (b), SA1.1–5 has only more gypsum peaks than that before corrosion, while the others have no obvious changes, indicating that AAC corrosion is not serious. Unlike AAC, the peaks of calcium silicate hydrate and $Ca(OH)_2$ in OPC disap-

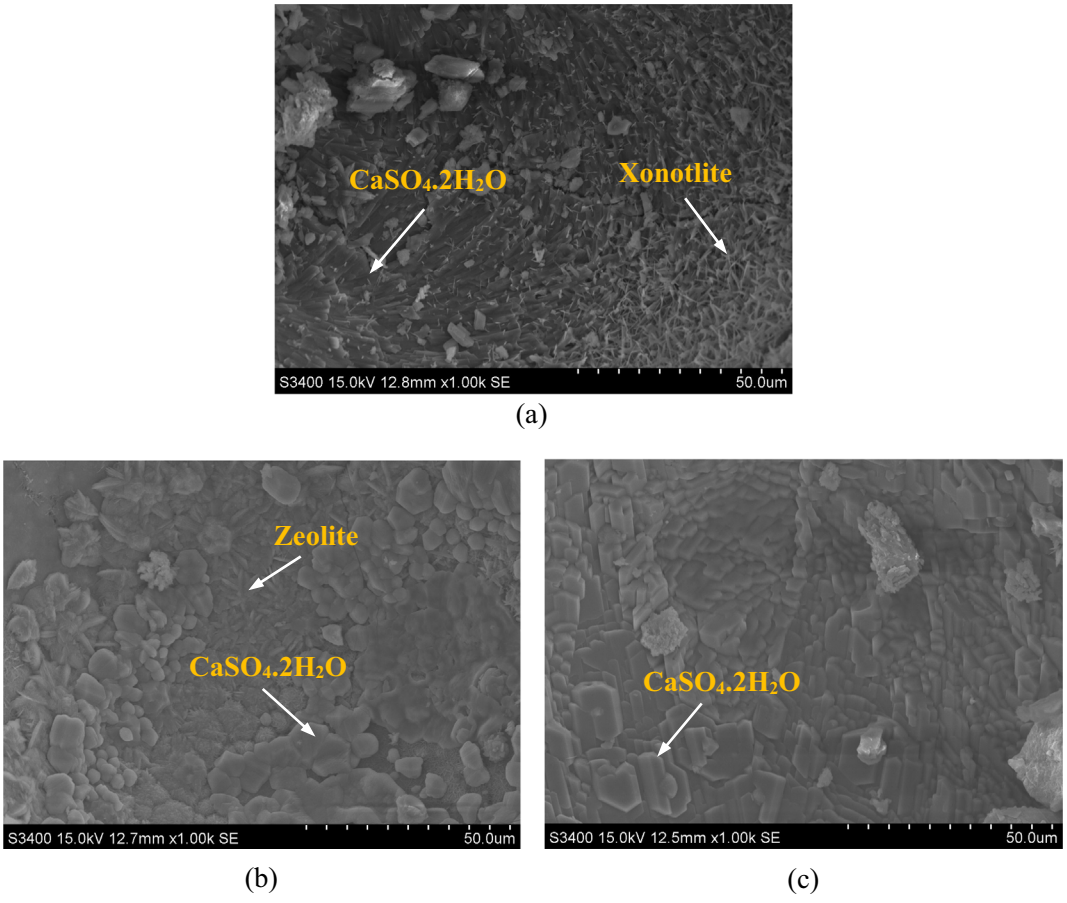

Fig. 13. Corrosion morphology of SA1.1.

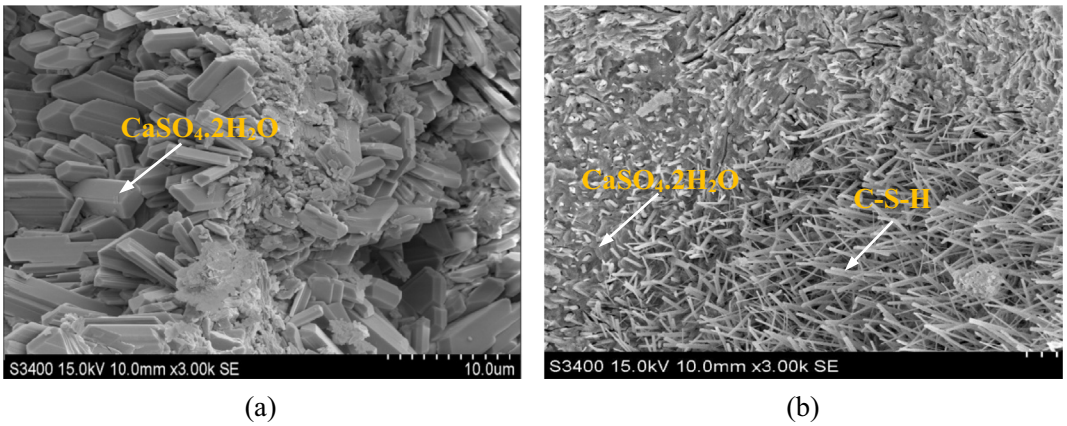

Fig. 14. Corrosion morphology of SP1.1.

pears and obvious gypsum peaks is produced. It can be concluded that the main hydration products of OPC have been destroyed and a great deal of gypsum has been produced. Therefore, compared with OPC, AAC is weakly destroyed by BSA and its main hydration products are not greatly affected.

4.7. FT-IR analysis

The effects of BSA corrosion on AAC and OPC under 56 days are qualitatively studied by FT-IR, as shown in Fig. 16. It shows the main bands at 455, 692, 780, 1002, 1112, 1432, 1637 and 3444 cm^{-1}. The stretching mode of Si-O in quartz [38] appears at 780 cm^{-1}. The Si-O bond [39,40] in the $[SiO_4]^{4-}$ tetrahedron of C-S-H appears at 1002 cm^{-1}. The bands at 455 and 692 cm^{-1} are Al-O bonds, which come from aluminosilicate [41–44]. The Ca-O bond is displayed in 1432 cm^{-1} band. The two broad absorption peaks at bands 3444 and 1637 cm^{-1} are respectively the tensile vibration of the hydroxide layer of Friedel salt and the hydrogen-bonded hydroxyl group of water molecules between the layers [45]. Before BSA corrosion, the infrared spectra of AAC are basically the same as that of OPC.

After BSA corrosion, for SA1.1–5, two new peaks appear at 1002 and 1114 cm^{-1}, indicating that the Si-O bond at 1002 cm^{-1} moves to the right, indicating that the original Si-O bond is damaged. At

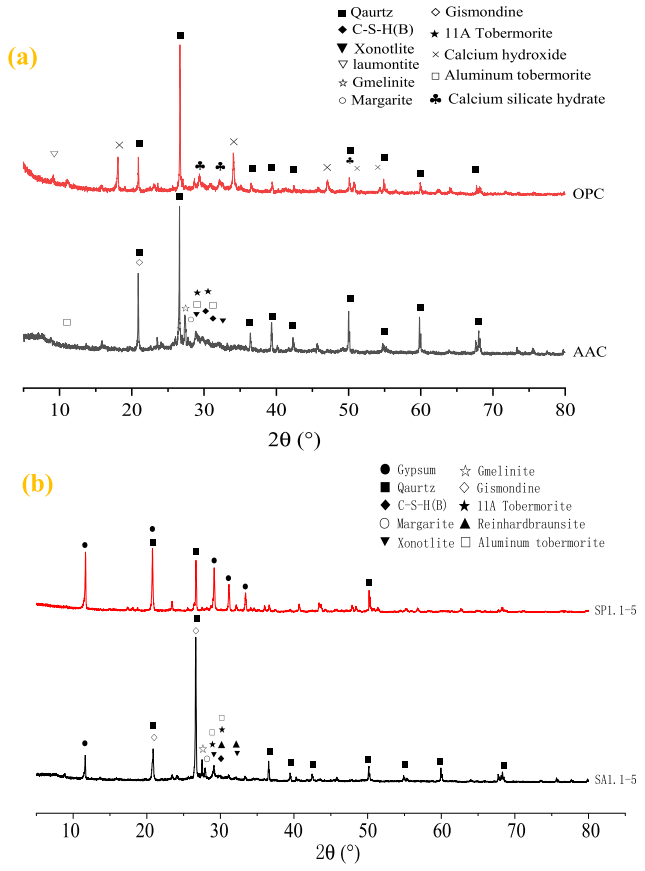

Fig. 15. XRD patterns of OPC and AAC: (a) Before BSA corrosion; (b) After BSA corrosion.

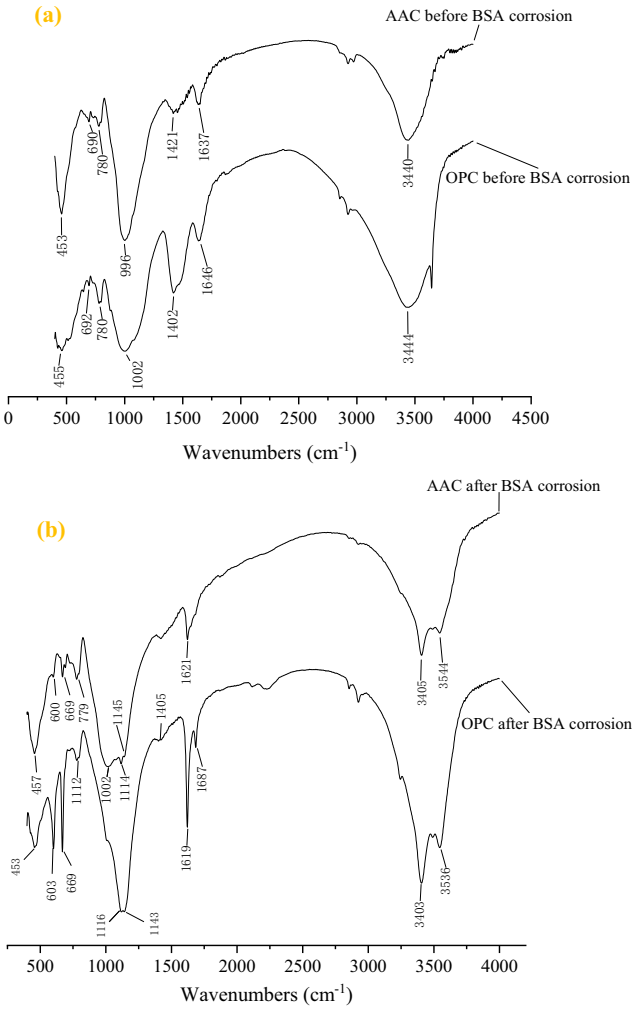

Fig. 16. FT-IR spectra of OPC and AAC: (a) Before BSA corrosion; (b) After BSA corrosion.

the same time, there is a small signal at 1145 cm^{-1} due to the carbonization reaction between carbon dioxide in the air and the sample, which is caused by calcium carbonate. The tensile mode of Si-O in 780 cm^{-1} quartz will not be changed by BSA corrosion. The Si-O bonds (996 cm^{-1}) and some Al-O bonds (453 and 690 cm^{-1}) are destroyed, resulting in new Si-O bonds (1002 and 1114 cm^{-1}) and Al-O bonds (600 and 669 cm^{-1}). However, these newly formed structures do not form other materials that contribute to structural strength [20]. The occurance of the stretching vibration of the S-O bond of SO_4^{2-} in dihydrate gypsum [46,47] is at bands 465, 515, 604, 669, 1119 and 1166 cm^{-1}, and the formation of the bands at 1621, 3405 and 3544 cm^{-1} are caused by the hydroxyl group in $CaSO_4{\cdot}2H_2O$ [46,48]. Moreover, it is shown that the absorption peaks at 1143 and 1687 cm^{-1} are only shown in OPC, which indicates that OPC has been consumed by H^+ under the erosion of BSA. On the other hand, after OPC is corroded by BSA, Ca-O band disappears at 1402 cm^{-1}, indicating that C-S-H had a serious decalcification effect. To some extent, it also indicates that OPC is subject to more serious corrosion than AAC. This is consistent with the results of Ca^{2+} emission test.

4.8. Discussion of corrosion mechanism

In the simulated BSA corrosion device, T.f bacteria convert H_2S into BSA in acidic medium. The main objects of BSA corrosion are hydrated calcium silicate and aluminosilicates. In fact, BSA has bacterial effects that chemical sulfuric acid does not have. Bacterial effects can be analyzed from the following aspects:

Firstly, there are many bacteria on the surface of the specimen. It can be seen from Fig. 10 that bacteria are not uniformly distributed on the surface of the test block, but selectively gathered on some protruding aggregates. This phenomenon also provides evidence for the gap between aggregate and slurry on the surface of concrete. Because of its poor acid resistance, the surface of OPC is quickly softened and a large amount of gypsum is produced. Compared with AAC, OPC provides more pore and gypsum, which is more conducive to bacterial growth and adhesion [11]. Therefore, OPC is more affected by bacteria than AAC.

Next, in terms of bacterial permeability, the volume of bacteria is about 1 μm [49], while the initial aperture of AAC and OPC are far less than 1 μm (see Table 4), so bacteria cannot penetrate into concrete under normal corrosion, and bacteria can only exist on the surface of concrete. It can also be seen from Fig. 11 that the internal structures of AAC and OPC are very compact except for the loose corrosion layer 1–2 mm away from the surface. In addition, the holes are sealed, and there are no cracks in the fracture surface. That is to say, bacteria cannot infiltrate into the interior of concrete.

In a word, in order to maintain the metabolic process of life, bacteria will produce acid continuously. BSA produced by bacteria will directly corrode the surface of concrete blocks, and keep the pH value of the surface of concrete blocks at the lowest level before death. The muddy gypsum corrosion layer produced by BSA in the process of corroding concrete creates good conditions for the growth of bacteria. Bacteria like to adsorb in wet gypsum environ-

ment. With the corrosion proceeding, the porosity of corrosive layer increases and becomes loose, more bacteria grow on the corrosive layer, more BSA is formed on the corrosive layer not far from the concrete of the non-corrosive layer, and infiltrates into the interior of the concrete, and reacts rapidly with the hydration products of the concrete to produce a large amount of gypsum. A lot of gypsum produces stress, which not only causes concrete cracking and accelerates ion of ion diffusion, but also promotes the dissolution of Ca-O, Si-O, and Al-O bonds in concrete by H^+. In addition, when bacteria produce BSA, besides SO_4^{2-} formed by transformation of S element, which is partly infiltrated into concrete, a large number of SO_4^{2-} from culture medium will also infiltrate into concrete continuously and participate in the corrosion of concrete. In brief, H^+ and SO_4^{2-} in the external solution can freely permeate into the surface of the uncorroded concrete from the corrosion layer to participate in the reaction, and the reactants can then diffuse to the external surface through the pore fluid in the pores.

It can be concluded from micro experiments that $Ca(OH)_2$ and C-S-H, the main hydration products in OPC, are seriously damaged and a large amount of gypsum is generated. For SA1.1, it was found in the XRD test results that the dispersion peak of calcium silicate hydrate disappeared, the Ca-O bond disappeared in the FT-IR test results, and a large amount of calcium elements in the corrosion layer were reduced in EDS test results, which indicated that calcium silicate hydrate was seriously damaged. In addition, a small amount of reinhardbraunsite and other substances were detected in XRD test results, that is, calcium silicate hydrates were decalcified after being corroded by BSA.

As one of the main hydration products in AAC, aluminosilicate substances (e.g. gmelinite and laumontite) are composed of tetrahedron $[SiO_4]^{4-}$ and $[AlO_4]^{5-}$, which are amorphous zeolites [50]. Allahverdi et al. [51,52] pointed out that the three-dimensional Si-O-Al bonded aluminosilicates framework is more durable in acidic media than fragile hydrated calcium silicate materials. In this paper, the corrosion mechanism under BSA for AAC includes leaching process, in which Na^+ and Ca^{2+} are exchanged by H^+ or H_3O^+ in solution, and electrophilic corrosion of Si-O-Al bond by acidic protons leads to the formation of new zeolite structure. Most notably, the Si-O bonds (996 cm^{-1}) and some Al-O bonds (453 and 690 cm^{-1}) are destroyed in the FT-IR test, generating new Si-O bonds (1002 and 1114 cm^{-1}) and Al-O bonds (600 and 669 cm^{-1}). These newly formed structures, however, do not form other materials that contribute to structural strength.

In addition, a large reduction of Ca^{2+} in the corrosion layer was observed in EDS test results, which also supported the evidence that Ca^{2+} was exchanged by H^+ ions. Section 4.3 shows that the amount of Ca^{2+} dissolved from OPC is larger than that dissolved from AAC. This is probably due to (a) more bacteria (see Fig. 10) adsorbed on the OPC surface than on the AAC surface, (b) the initial average pore size of OPC is larger than that of AAC (see Table 4), (c) the corrosion depth of OPC is greater than that of AAC (see Fig. 11). Therefore, it is presumed that BSA infiltrated into OPC may be more than AAC, which may lead to the increase of porosity in the corroded layer of OPC than that in the corroded layer of AAC. The increase rate of porosity in the corrosive layer of OPC is larger than that of AAC, which leads to the change rate of diffusion coefficient in the corrosive layer of OPC is larger than that in the corrosive layer of AAC [53].

As confirmed by appearance change, mass loss, Ca^{2+} emission, X-ray diffraction, Fourier transform infrared spectroscopy, and environmental scanning electron microscopy analyses, the corrosion resistance of AAC to BSA is better than that of OPC, it was probably due to shortening the pathway of BSA to erode OPC.

5. Conclusions

1. Under the corrosion of BSA, AAC has a lower apparent corrosion degree than OPC, while the gypsum layer of OPC is obviously softer and more gypsum is produced. And the dissolution of calcium ions, the loss rate of compressive strength and mass of OPC are higher than those of AAC.
2. Bacteria does not distribute uniformly on the surface of the test block, but clustered together showing an uneven cluster distribution. The number of bacteria attached to the surface of OPC is higher than that of AAC. Under BSA erosion, the main corrosion product of OPC and AAC is gypsum, and the amount of gypsum produced by OPC is larger than that of AAC. The bacterial effect on the surface of OPC corrosion layer is greater than that of AAC, which probably shorten the BSA corrosion path of OPC. Therefore, the corrosion of OPC is more serious than that of AAC.
3. By analyzing the corrosion samples 5 mm away from the surface of the test block, it can be seen that the main hydration products of OPC, $Ca(OH)_2$ and C-S-H, are destroyed and produce a large amount of gypsum, while AAC is weakly destroyed by BSA and its main products are not greatly affected. Therefore, AAC is much more resistant to BSA than OPC. Moreover, the concentration of BSA has no effect on the corrosion mechanism of OPC and AAC.

Declaration of Competing Interest

We confirm that there are no known conflicts of interest associated with this publication and there has been no significant financial support for this work unlisted that have influenced its outcome.

Acknowledgements

The funding of this study came from the National Nature Science Foundation of China (NSFC) (Approval No. 51708120, 51479036, 51878179 and 51708119). Thanks to all the anonymous reviewers for helping improve this article.

References

[1] G. Jiang, M. Zhou, T.H. Chiu, et al., Wastewater-enhanced microbial corrosion of concrete sewers, Environ. Sci. Technol. 50 (15) (2016) 8084–8092.
[2] J. Vollertsen, A.H. Nielsen, H.S. Jensen, et al., Corrosion of concrete sewers-The kinetics of hydrogen sulfide oxidation, Sci. Total Environ. 394 (1) (2008) 162–170.
[3] T.M. Wahshat, Sulfur Mortar and Polymer Modified Sulfur Mortar Lining for Concrete Sewer Pipe, Iowa State University, Ames Iowa, 2001.
[4] C.D. Parker, The corrosion of concrete-isolation of a species of bacterium associated with the corrosion of concrete exposed to atmospheres containing hydrogen sulfide, Exp. Biol. Med. Sci. 23 (3) (1945) 14–17.
[5] D. Walsh, D. Pope, M. Danford, et al., The effect of microstructure on microbiologically influenced corrosion, JOM-J. Miner. Met. Mater. Soc. 45 (9) (1993) 22–30.
[6] F.E. Kulman, Microbiological corrosion of buried steel pipe, Corrosion 9 (1) (1953) 11–18.
[7] E. Heitz, H.-C. Flemming, W. Sand, Microbially Influenced Corrosion of Materials: Scientific and Engineering Aspects, Springer-Verlag, Berlin, New York, 1996.
[8] C.D. Parker, The corrosion of concrete, Immunol. Cell Biol. 23 (2) (1945) 91–98.
[9] J.M. Tulliani, L. Montanaro, A. Negro, et al., Sulfate attack of concrete building foundations induced by sewage waters, Cem. Concr. Res. 32 (6) (2002) 843–849.
[10] F. Rendell, R. Jauberthie, The deterioration of mortar in sulphate environments, Constr. Build. Mater. 13 (6) (1999) 321–328.
[11] J. Monteny, E. Vincke, A. Beeldens, et al., Chemical, microbiological, and in situ test methods for biogenic sulfuric acid corrosion of concrete, Cem. Concr. Res. 30 (4) (2000) 623–634.
[12] T. Mori, T. Nonaka, K. Tazaki, Interactions of nutrients, moisture, and pH on microbial corrosion of concrete sewer pipes, Water Res. 26 (1) (1992) 29–37.
[13] J. Skalny, J. Marchand, I. Odler, Sulfate Attack on Concrete, Spon Press, London, 2002.

[14] J.L. Davis, D. Nica, K. Shields, et al., Analysis of concrete from corroded sewer pipe, Int. Biodeterior. Biodegrad. 42 (1) (1998) 75–84.
[15] C. Chen, T. Ji, Y. Zhuang, et al., Workability, mechanical properties and affinity of artificial reef concrete, Constr. Build. Mater. 98 (2015) 227–236.
[16] M.T. Bassuoni, M.L. Nehdi, Resistance of self-consolidating concrete to sulfuric acid attack with consecutive pH reduction, Cem. Concr. Res. 37 (7) (2007) 1070–1084.
[17] E. Vincke, E.V. Wanseele, J. Monteny, et al., Influence of polymer addition on biogenic sulfuric acid attack of concrete, Int. Biodeterior. Biodegrad. 49 (4) (2002) 283–292.
[18] J. Hill, E.A. Byars, J.H. Sharp, et al., An experimental study of combined acid and sulfate attack of concrete, Cem. Concr. Compos. 25 (8) (2003) 997–1003.
[19] Y.Y. Wei, J. Luo, Y. Xiao, et al., Study on acid erosion test of cement mortar I non-flowing acid water erosion test, J. Chin. Ceram. Soc. 26 (3) (1998) 417–423.
[20] Y. Xie, X. Lin, W. Pan, et al., Study on corrosion mechanism of alkali-activated concrete with biogenic sulfuric acid, Constr. Build. Mater. 188 (2018) 9–16.
[21] Y. Yang, T. Ji, X. Lin, et al., Biogenic sulfuric acid corrosion resistance of new artificial reef concrete, Constr. Build. Mater. 158 (2018) 33–41.
[22] C. Shi, P. Krivenko, D. Roy, Alkali-Activated Cement and Concrete, Taylor & Francis, London and New York, 2006.
[23] R.E. Beddoe, H.W. Dorner, Modelling acid attack on concrete: Part I. The essential mechanisms, Cem. Concr. Res. 35 (12) (2005) 2333–2339.
[24] W. Jiang, M.R. Silsbee, E. Breval, et al., Alkali activated cementitious materials in chemically aggressive environments, in: K.L. Scrivener, J.F. Young (Eds.), Mechanisms of Chemical Degradation of Cement-Based Systems, E & FN Spon, London, 1997, pp. 289–296.
[25] P. Sun, H.C. Wu, Chemical and freeze-thaw resistance of fly ash-based inorganic mortars, Fuel 111 (9) (2013) 740–745.
[26] GB/T14684-2001, Sand for construction, General Administration of Quality Supervision, Inspection and Quarantine of the PRC, 2001.
[27] GB/T14685-2001, Pebbie and crushed stone for building, General Administration of Quality Supervision, Inspection and Quarantine of the PRC, 2001.
[28] R.E. Buchanan, N.E. Gibbons, Bergey's Manual of Determinative Bacteriology, nineth ed., Williams and Wilkins, Baltimore, Maryland, 1994.
[29] R.L. Islander, J.S. Devinny, F. Mansfeld, et al., Microbial ecology of crown corrosion in sewers, J. Environ. Eng.-ASCE. 117 (6) (1991) 751–770.
[30] People's Republic of China Ministry of Housing and Urban-rural Development, in: JGJ 55-2011 Specification for Mix Proportion Design of Ordinary Concrete. Beijing: China Building Industry Press, 2011.
[31] W. Sand, E. Bock, D. White, Importance of hydrogen Sulfide, Thiosulfate, and Methylmercaptan for Growth of Thiobacilli during Simulation of Concrete Corrosion, Appl. Environ. Microbiol. 53 (7) (1987) 1645–1648.
[32] T. Mori, M. Koga, Y. Hikosaka, et al., Microbial corrosion of concrete sewer pipes, H_2S production from sediments and determination of corrosion rate, Water Sci. Technol. 23 (7–9) (1991) 1275–1282.
[33] T. Mori, T. Nonaka, K. Tazaki, et al., Interactions of nutrients, moisture and pH on microbial corrosion of concrete sewer pipes, Water Res. 26 (1) (1992) 29–37.
[34] Ministry of Construction, The state administration of quality supervision, in: Inspection and Quarantine People's Republic of China. GB/T50081-2002 Standard for test method of mechanical properties on ordinary concrete.
[35] F. Pacheco-torgal, Alkali-activated binders: A review-Part 1. Historical background, terminology, reaction mechanisms and hydration products, Constr. Build. Mater. 22 (2008) 1305–1314.
[36] L.D. Windt, P. Devillers, Modeling the degradation of Portland cement pastes by biogenic organic acids, Cem. Concr. Res. 40 (8) (2010) 1165–1174.
[37] M.G. Alexander, C. Fourie, Performance of sewer pipe concrete mixtures with portland and calcium aluminate cements subject to mineral and biogenic acid attack, Mater. Struct. 44 (1) (2011) 313–330.
[38] A. Fernández-Jiménez, A. Palomo, Mid-infrared spectroscopic studies of alkali-activated fly ash structure, Microporous Mesoporous Mat. 86 (3) (2005) 207–214.
[39] P. Yu, R.J. Kirkpatrick, B. Poe, et al., Structure of calcium silicate hydrate (C-S-H): Near-, mid-, and far-infrared spectroscopy, J. Am. Ceram. Soc. 82 (82) (2010) 742–748.
[40] M.Y.A. Mollah, F. Lu, D.L. Cocke, An X-ray diffraction (XRD) and Fourier transform infrared spectroscopic (FT-IR) characterization of the speciation of arsenic (V) in Portland cement type-V, Sci. Total Environ. 224 (3) (1998) 57–68.
[41] D.W. Breck, Zeolite Molecular Sieves, Krieger, 1984.
[42] T. Bakharev, Resistance of geopolymer materials to acid attack, Cem. Concr. Res. 35 (4) (2005) 658–670.
[43] F. Puertas, S. Martínez-Ramírez, S. Alonso, et al., Alkali-activated fly ash/slag cement-Strength behaviour and hydration products, Cem. Concr. Res. 30 (10) (2000) 1625–1632.
[44] M.A.M. Ariffin, M.A.R. Bhutta, M.W. Hussin, et al., Sulfuric acid resistance of blended ash geopolymer concrete, Constr. Build. Mater. 43 (2013) 80–86.
[45] G.R. Qian, J. Shi, Y.L. Cao, et al., Properties of MSW fly ash-calcium sulfoaluminate cement matrix and stabilization/solidification on heavy metals, J. Hazard Mater. 152 (1) (2008) 196–203.
[46] S.C.B. Myneni, S.J. Traina, G.A. Waychunas, et al., Vibrational spectroscopy of functional group chemistry and arsenate coordination in ettringite, Geochim. Cosmochim. Acta. 62 (62) (1998) 3499–3514.
[47] Y.C. Nagar, M.D. Sastry, B. Bhushan, et al., Chronometry and formation pathways of gypsum using Electron Spin Resonance and Fourier Transform Infrared Spectroscopy, Quat. Geochronol. 5 (6) (2010) 691–704.
[48] N. Kybartien, V. Leskevivien, Z. Valancius, Influence of Ce^{3+} on the formation of a-Semi-Hydrate Gypsum, Mater. Sci. 18 (4) (2012) 385–389.
[49] A.R. Colmer, M.E. Hinkle, The role of microorganisms in acid mine drainage: a preliminary report, Science 106 (2751) (1947) 253–256.
[50] P. Duxson, A. Fernández-Jiménez, J.L. Provis, et al., Geopolymer technology: the current state of the art, J. Mater. Sci. 42 (9) (2007) 2917–2933.
[51] A. Allahverdi, F. Škvára, Nitric acid attack on hardened of geopolymeric cements Part I, Ceram. Silik. 45 (3) (2001) 81–88.
[52] A. Allahverdi, F. Škvára, Nitric acid attack on hardened paste of geopolymeric cement; Part 2, Ceram. Silik 4 (45) (2001) 143–149.
[53] M. Mainguy, C. Tognazzi, J.M. Torrenti, et al., Modelling of leaching in pure cement paste and mortar, Cem. Concr. Res. 30 (1) (2000) 83–90.